Thesis for the Degree of Master of Engineering

Rice starch coated iron oxide nanoparticles: A theranostic probe for photoacoustic imaging-guided photothermal cancer therapy

By

Vo Thi Mai Thien

Department of Industry 4.0 Convergence Bionics Engineering

The Graduate School

Pukyong National University

August 2021

Rice starch coated iron oxide nanoparticles: A theranostic probe for photoacoustic imaging-guided photothermal cancer therapy

(쌀 전분 코팅 산화철 나노 입자 : 광 음향 영상 유도 광열 암 치료를 위한 치료 탐침)

Advisor: Prof. Junghwan Oh

by

Vo Thi Mai Thien

A thesis submitted in partial fulfillment of the requirements for the degree of

Master of Engineering

In Department of Industry 4.0 Convergence Bionics Engineering

The Graduate School

Pukyong National University

August 2021

Rice starch coated iron oxide nanoparticles: A theranostic probe for photoacoustic imaging-guided photothermal cancer therapy

쌀 전분 코팅 산화철 나노 입자 : 광 음향 영상 유도 광열 암 치료를 위한 치료 탐침

A dissertation

By

Vo Thi Mai Thien

Approved by:

Prof. Joong Ho Shin, Ph.D.
(Chairman)

Prof. Hae Gyun Lim, Ph.D.
(Member)

Prof. Junghwan Oh, PhD.
(Member)

August 27, 2021

LIST OF CONTENTS

LIST OF FIGURES

LIST OF TABLES

Rice starch coated iron oxide nanoparticles: A theranostic probe for photoacoustic imaging-guided photothermal cancer therapy

Vo Thi Mai Thien

Department of Industry 4.0 Convergence Bionics Engineering,
The Graduate School, Pukyong National University

Abstract

In recent years, suitable bioactive materials coated nanoparticles have attracted substantial attention in the field of biomedical applications. The present study emphasizes experimental details for the synthesis of boiling rice starch extract (BRE) coated iron oxide nanoparticles (IONPs) to treat cancer by photoacoustic imaging (PAI)-guided chemo-photothermal therapy. The solvothermal method was used to synthesize IONPs. The physical immobilization method helps to coat BRE-loaded doxorubicin (DOX) molecules on the iron oxide surface. In vitro drug release was estimated in basic (pH 9.0), neutral (pH 7.2), and acidic (pH 4.5) media for varying time periods using ultraviolet-visible spectroscopy. The chemical and physical properties of the synthesized spherical BRE-IONPs were characterized using sophisticated analytical instrumentation. A magnetic saturation experiment was performed with BRE-IONPs for evaluating possible hyperthermia in targeted drug delivery. The biological activity of the synthesized BRE-IONPs was investigated by the 3-(4,5-dimethylthiazol-2-yl)-2,5-diphenyl tetrazolium bromide assay and acridine orange/propidium iodide fluorescence cell viability study. BRE-IONPs showed excellent photothermal stability, with a high photothermal conversion efficiency ($\eta = 29.73$ %), biocompatible property, and high near-infrared region absorption for PAI-guided PTT treatment. This study will provide a better

understanding of rice starch as a suitable bioactive coating material for possible theranostic applications.

Keywords: Iron oxide, Drug delivery, cancer treatment, photothermal therapy, photoacoustic imaging

Chapter 1. Introduction

In recent years, iron oxide nanoparticles (IONPs) have been investigated for multifunctional biomedical applications, including targeted drug delivery [1], magnetic resonance imaging [2], photothermal therapy (PTT) [3], magnetic separation [4], and diagnostics [5]. Due to their unique properties, such as lower toxicity, biocompatible properties, active magnetic properties, chemical stability, and bioactive nature [6, 7], IONPs are widely used for various clinical applications. There are eight well-known iron oxides (IOs) in nature [8], and among them, magnetite (Fe_3O_4), maghemite (γ-Fe_2O_3), and hematite (α-Fe_2O_3) show unique magnetic properties. Fe_3O_4 and γ-Fe_2O_3 are ideal materials for nonmedical and clinical applications. IONPs are the primary choice for anticancer drug delivery because of their controlled magnetic response towards external magnetic fields at the target site, without affecting non-target specific regions [9]. However, Fe_3O_4 nanoparticles without any biocompatible coating have several limitations for biomedical applications, which results in free radicals generation [10], ineffective binding of the ligand, drug delivery failure [11], and instability inside body system [12]. These challenges could easily be improved by a suitable biocompatible coating over Fe_3O_4 nanoparticles surface [13].

Bioactive materials offer several advantages with different functional groups for enhanced drug interactions, with high drug loading capabilities and encapsulation efficiency [14]. Studies have demonstrated different types of ligands used for IONPs functionalizationsome of these include starch, dextran, gelatin, alginate, chitosan, albumin, polyethylene glycol, polyvinyl alcohol, polyvinyl pyrrolidone, and polylactic-co-glycolic acid [15-20]. Reports on coating materials have suggested a favorable conjugation of drugs on the IONPs surface with high in situ retention time [21]. Moreover, the surface modifications of IONPs by bioactive materials offers

other advantages, including enhanced in vivo circulation evading efficiency due to steric stabilization and improvement in the binding ability of biological moieties, such as proteins, lipids, enzymes, antibodies, DNA, and RNA. Among these bioactive materials, specifically starch have gained attention due to its non-toxic, biocompatible, biodegradable properties [22]. Although, certain innate characteristics of raw starch, including less solubility, agglomeration, poor powder flow, adhesive nature, and high viscosity limits its performance for targeted drug delivery applications [23]. To overcome these limitations, bioactive materials have been the primary choice of interest of all researchers. Boiling rice extract or rice starch possesses numerous negatively-charged functional groups (CH_2COO-), which enables drug loading and interaction on its surface [24]. BRE is an economical, renewable and biodegradable carbohydrate, comprising a large number of glucose units linked by glycosidic bonds [25]. The use of BRE as a coating agent with biodegradable, hydrophilic property with photoacoustic imaging guided photothermal cancer therapeutic efficacy has rarely been reported so far. The BRE coating may achieve stable, relatively mono-disperse particles for drug delivery with improved drug bio-functionality [26]. The functionalized BRE molecule could be an attractive support for various colloidal metal nanoparticles. Jia Yang et al. showed the application of IONPs with different materials coatings for PTT. In this study, IONPs were coated with polyacrylic acid, PVA, and polyethyleneimine using a mild reduction route to investigate their usability as a photothermal agent. Jia Yang et al. used a high laser power density of 1.6 W/cm^2, which is higher than the US Federal Laser Product Performance Standard for skin tolerance [27]. Mohapatra et al. used rice starch to coat IONPs for drug delivery applications only [28]. However, in the present study, we emphasized the use of BRE-coated IONPs for multimodal drug delivery, photoacoustic imaging (PAI), and PTT treatment.

Another study reported that the rice starch (BRE) can be utilized for coating and stabilizing IONPs, thereby improving IONPs' ability to effectively bind and load

doxorubicin (DOX), an anticancer drug molecule, via an electrostatic interaction [29]. Fe_3O_4 nanoparticles were synthesized via a solvothermal route, which was further modified by BRE coating. Different analytical techniques were employed to characterize the synthesized nanoparticles for explaining the advanced nanostructure of BRE-coated IONPs (BRE-IONPs). The synthesized IONPs and BRE-IONPs cytotoxicity experiment was performed using MG-63 osteoblast cell lines. BRE-IONPs were further studied using drug loading and releasing experimental study. The resulting nanoparticles showed strong photothermal effect under 808 nm near-infrared (NIR) laser irradiation. Additionally, the phantom study of PAI in association with BRE-IONPs revealed a strong photoacoustic (PA) signal emission for bioimaging. Moreover, the PAI phantom experiment was performed using DOX-BRE-IONPs, which revealed an excellent PA signal. These high-quality PA signals may be useful for biomedical imaging purposes. The 3-(4,5-dimethylthiazol-2-yl)-2,5-diphenyl tetrazolium bromide (MTT) assay revealed that BRE-IONPs exhibited nontoxic behavior. These findings inspire the impending application of BRE-IONPs as a promising material for multifunctional biomedical applications as shown in Figure 1.

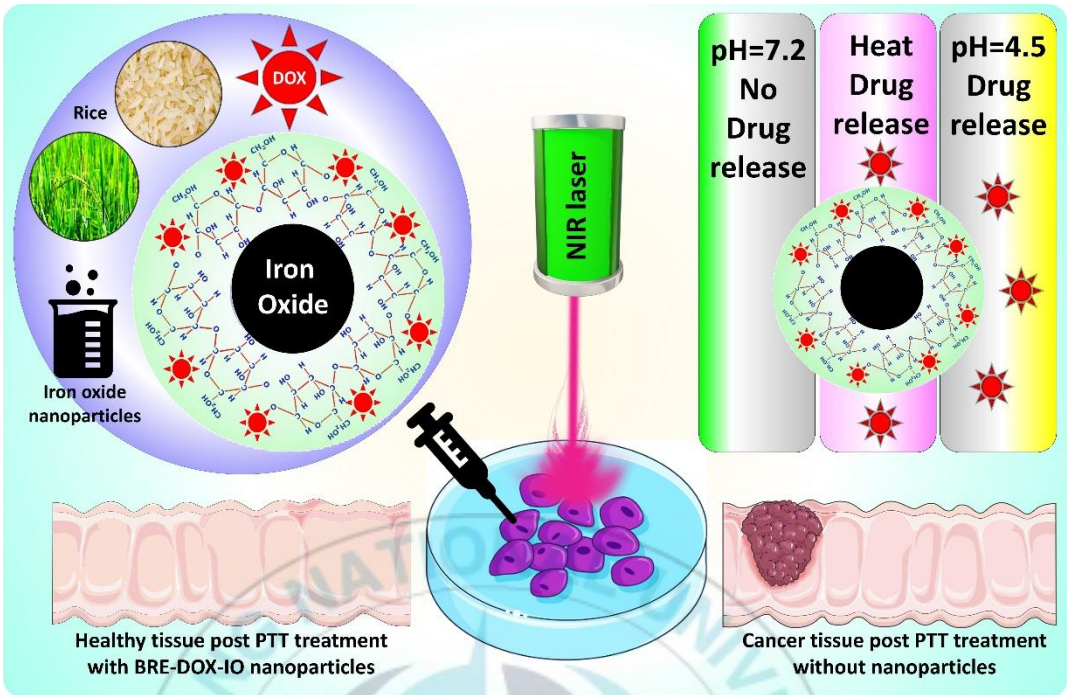

Figure 1: Schematic representation of DOX-BRE-IONPs for its potential drug delivery and biomedical applications.

Chapter 2. Experimental

1. Materials

Iron (III) chloride hexahydrate ($FeCl_3.6H_2O$), ethylene glycol, Sodium acetate (NaOAc), trisodium citrate, 3-(4, 5-dimethythiazol- 2-yl)-2, 5-diphenyl tetrazolium bromide [MTT], Acridine Orange, Propidium Iodide Stain were purchased from Sigma Aldrich, USA. All the chemicals were used without any further purification. The Vietnamese rice (*Oryza sativa*) was procured from online Korean G-market.

2. Synthesis of magnetic IONPs

Fe_3O_4, nanoparticles were synthesized using the solvothermal method [30]. First, 1.621 g $FeCl_3.6H_2O$ was dissolved in 60 mL ethylene glycol with magnetic stirring under nitrogen atmosphere for 30 min. Next, 0.98 g sodium acetate was added under continuous vigorous stirring. An amount of 0.5 g trisodium citrate was added into the above solution under continuous magnetic stirring for 1 h, at ambient temperature. The final mixture was transferred to a Teflon-coated stainlesssteel autoclave chamber (100 mL capacity) and heated at 185 °C for 12 h. Then, the autoclave chamber was cooled down to ambient temperature, and the obtained dark black precipitate was repeatedly washed thoroughly with ethanol. The washed nanoparticles were dried at 50 °C for 8 h and stored for further experimental study.

3. Preparation of BRE

To prepare BRE, 50 g of Vietnamese rice was initially washed several times with distilled water. In a 250-mL beaker, 100 mL DI water was added to the washed rice and boiled for 30 min. Next, the cooled white rice extract was collected. The collected rice extract was then filtered using Whatman filter paper and stored for future use. No additional chemicals or preservatives were used. For all experiments, we used only freshly prepared BRE.

4. Synthesis of BRE-IONPs and DOX-BRE-IONPs

The synthesized IONPs are highly stable and were used for BRE coating and freshly prepared BRE was used to coat IONPs. First, 100 mg synthesized IONPs were placed in a 15-mL tube. Next, 10 mL fresh BRE was added to IONPs and subjected to vigorous shaking for 3 h. The BRE-IONPs solution was placed on a 30-mm plate and concentrated in a hot air oven at 40 °C overnight. Finally, after drying, the BRE-IONPs flakes were collected and mildly ground using an agate mortar pestle. The synthesized material was marked as BRE-IONPs.

To synthesize DOX-loaded BRE-IONPs, we followed a previous method and added 1 mL 0.002 M DOX to the BRE-IONPs solution. The DOX-BRE-IONPs system was subjected to vigorous shaking for 24 h and then dried in the hot air oven for 24 h. Finally, after complete drying, the nanoparticle system was gently ground using an agate mortar pestle and further studied for biomedical applications. The performance of drug-loaded DOX-BRE-IONPs was evaluated using ultraviolet-visible (UV-vis) spectroscopy.

5. DOX-releasing kinetics of BRE-IONPs

The in vitro drug release behavior of DOX-loaded BRE-IONPs was evaluated using 20 mg DOX BRE-IONPs in a dialysis membrane molecular weight cut-off (MWCO) 12 kDa at a physiological body temperature (37 °C) under different pH values (9, 7.2, and 4.5). The dialysis membrane bags were transferred in 10 mL phosphate buffered saline (PBS) solution under three pH conditions with stirring. The drug release kinetics were measured at time intervals of 2 h for the first 24h and consequently at time intervals of 12 h until 48 h.

6. Biological study for cell cytotoxicity

6.1 MTT assay

A standard MTT toxicity assessment was performed to study the toxicity of IONPs, BRE-IONPs, and DOX-BRE-IONPs on MG-63 cells. First, MG-63 cell lines were seeded on 96 multi-well plates at a concentration of 10^4 cells/well at 37 °C and 5% CO_2 atmospheric condition. After 24 h incubation, the cells were exposed to the synthesized IONPs, BRE-IONPs, and DOX-BRE-IONPs for 24 h, at concentrations of 50, 100, 150, 200, and 250 μg/mL. For the time-dependent toxicity study, IONPs, BRE-IONPs, and DOX-BRE-IONPs (200 μg/mL each) were exposed for 24, 48, and 72 h, respectively. MG-63 cells without any nanoparticles were used as the control. Thereafter, the cells were cultured in 100 μL MTT reagent (0.5 mg/mL) for 4 h in a CO_2 incubator. After discarding the media, 100 μL dimethyl

sulfoxide (DMSO) was added for 15 min to dissolve the purple formazan crystals [31]. The intensity of the purple formazan was measured using a 570-nm microplate reader (Tecan, Infinite F50). The results of the in vitro cell cytotoxic efficiency study were calculated as percentages using the following formula (the control group is considered to have 100% cell viability):

$$\textbf{\textit{Viable cells}}\ (\%) = \frac{\textbf{\textit{Absorbance of treated cells}}}{\textbf{\textit{Absorbance of controlled cells}}}\ X\ 100$$

6.2 Fluorescence staining (acridine orange/propidium iodide [AO/PI])

Cell viability experiments were performed using the AO and PI stains. MG-63 cells (10^4 cells/well) were seeded in 12-well cell culture plates and incubated. The cells were treated with 200 μg/mL BRE-IONPs, with a treatment period was 24, 48, and 72 h. The control wells did not contain any nanoparticles. After incubation, the treated cells were stained with 100 μL of AO and PI for 10 min (stock concentration, 1 μg/mL). In the final step, cells were washed with PBS solution and analyzed under 20 × and 40 × magnifications using LEICA DMI 3000B (Germany) fluorescence microscope under a 450-490 nm filter.

7. Characterization

The synthesized biocompatible BRE-IONPs and IONPs were characterized by powder X-ray diffraction (XRD, Bruker AXN diffractometer) using Cu Kα radiation (λ = 0.15405 nm) at 40 kV/40 mA. The absorption spectra of sample solutions were recorded by using a UV–vis spectroscopy (Thermo Biomate 5 Spectrophotometer). Fourier-transform infrared (FTIR, JASCO FRIT 4100) spectroscopy using KBr pellets and Raman spectroscopy (JASCO (NRS-5100) using a 632.8 nm He-Ne laser were performed to study functional and structural groups. Thermogravimetric and differential thermal analysis (TG-DTA, Perkin Elmer Pyris Diamond) was performed at a heating rate of 10 °C/min in air atmosphere. Furthermore, to study morphology, shapes and elemental compositions,

Field emission transmission electron microscopic, (FE-TEM, JEOL JEM-2010 microscope, Japan), with energy dispersive spectroscopy (EDS) analyses were employed. The zeta potential of BRE, BRE-IO, DOX-BRE-IONPs at different pH level was measured by using Anton Paar Litesizer^{TM} 500 instrument. The magnetic saturation study was performed by superconducting quantum interference device magnetometer (Quantum design, MPMS XL, USA). An 808 nm NIR laser with continuous-wave (CW) pulse from Hi-Tech Optoelectronics Co. (Beijing, China) was used on all photothermal related experimental study. Thermometer (MASTECH, CA, USA) was used to record temperature of laser irradiated solutions via a thermal fiber. A FLIR i5 infrared (IR) camera (FLIR-Systems Inc., Portland, USA) was used to capture thermal photos. Fluorescent images were taken using a fluorescent microscope (Leica Microsystems GmbH, Wetzlar, Germany).

8. Heating effect evaluation

The synthesized nanoparticles were further studied for heat generation in a photothermal conversion experiment. In this experiment, the IONPs, BRE-IONPs, and DOX-BRE-IONPs were dispersed in water with a certain concentration. From the prepared solution, 1 mL nanoparticle suspension was added in 12-well cell culture plate. The plate was exposed to 1.0 W/cm^2 NIR laser light uninterruptedly for 5 min. After laser irradiation, a thermal probe was used to record the temperature changes in the solution. Repeated laser irradiation (on and off laser) experiments were performed to evaluate the photothermal stability of DOX-BRE-IONPs. DOX-BRE-IONPs (200 μg/mL) were irradiated under a 1.0 W/cm^2 808 nm NIR laser until it achieved the highest temperature. Finally, the suspension was removed and left to naturally cool to ambient temperature. The heating and cooling cycles of the repeated laser irradiation experiment was performed for five times, and the temperature of the DOX-BRE-IONPs solution was continuously monitored using a thermometer probe. The photothermal conversion efficiency of DOX-BRE-IONPs was calculated as $\eta = 29.73$ %, which is sufficient to treat cancer cells.

9. In vitro photothermal therapy

For in vitro photothermal therapy, the MG-63 cell line was seeded at a concentration of 10^4 cells/well in a 12-well plate. After 24 h incubation, the cells were treated with IONPs, BRE-IONPs, and DOX-BRE-IONPs at a concentration of 200 μg/mL. After 6 h incubation, the cells were washed with PBS and again added to fresh Dulbecco's modified Eagle medium. Next, the cells were exposed to the 1.0 W/cm^2 808 nm NIR laser for 5 min. After thermal treatment, cells were collected by scrapping and incubated with 100 μl MTT reagent for 4 h. Finally, the solution was decanted, and 500 μl DMSO was added. After 20-min incubation, the cells were mixed by aspiration using a 500 μl pipette and finally placed in a 96 well plate. Cell solution (300 μl) was added to each well and observed under 570 nm wavelength in the TECAN plate reader.

After treatment, AO/PI fluorescence study was performed to imagine live/dead cells. The cells were seeded in a 12-well plate (10^4 cells/well) and classified into four groups: PBS plus NIR laser (group I), IONPs plus NIR laser (group II), BRE-IONPs plus NIR laser (group III), and DOX-BRE-IONPs plus NIR laser (group IV). The cells were incubated with 200 μg/mL IONPs, BRE-IONPs, and DOX-BRE-IONPs for 4 h, and the cells in the four groups were irradiated with the 1.0 W/cm^2 808-nm NIR laser for 5 min. After 2 h incubation, the cells were stained with AO and PI. Finally, the cells were observed under a fluorescence microscope.

10. In vitro photoacoustic imaging

The photoacoustic imaging was performed using an indigenously developed PAI system (Ohlabs Corp. Busan, Republic of Korea). Various concentrations of DOX-BRE-IONPs solutions (25, 50, 100, 200, and 400 μg/mL) were incubated with MG-63 cells for 24 h. After incubation, the cells were washed twice with PBS to remove excess nanoparticles and dead cell. Finally, the attached cells were collected by scrapping and loaded onto a 150-μl Polytetrafluoroethylene (PTFE) tube (1.6

mm inner diameter). After loading, the tube was sealed on both sides using silicone, and the prepared phantoms were placed in the PAI machine.

Chapter 3. Results and discussion

1. X-ray diffraction (XRD) analysis

The XRD peaks of the synthesized IONPs revealed high crystallinity, as shown in Fig. 1a. The characteristic adsorption peaks for IONPs marked at 2θ = 30.4°, 35.1°, 43.3°, 53.7 °, 57.4°, and 62.9° corresponding to 220, 311, 400, 422, 511, and 440, respectively, were well resolved in the XRD graph. These six diffraction peaks are consistent with the standard pattern for crystalline magnetite with a cubic inverse spinel structure. The XRD of pristine magnetite IONPs, BRE-IONPs, and DOX-BRE-IONPs are represented in Figure 2a, b, and c, respectively. No crystalline sharp peaks were observed for BRE-IONPs and DOX-loaded BRE-IONPs. The concentration of IONPs in BRE-IONPs and DOX-BRE-IONPs was very low. Moreover, BRE is a natural rice starch material that coats IONPs. Because of the amorphous structure of BRE, the sharp XRD peaks for IONPs were submerged. No big differences were observed in XRD peaks for BRE-IONPs and DOX-BRE-IONPs. This indicates peak broadening with increasing BRE concentration around the IO core due to a decrease in the crystallite size [10]. For IONPs, a powdered sample was analyzed; DOX-BRE-IONPs was cast on a glass plate, and the cast thin-film sample was characterized under XRD. In XRD analysis, we could not find any specific peaks for the BRE-modified sample.

2. UV–vis spectra analysis

The synthesized IONPs, BRE-IONPs, and DOX-BRE-IONPs were studied using UV–vis absorption spectroscopy (Figure 2d). The absorption spectra were recorded in the 325–900 nm range. UV-vis spectroscopy revealed a peak at 480–510 nm, which is relevant to DOX molecules. DOX-BRE-IONPs showed an absorption peak at approximately 360–400 nm and a small absorption hump at approximately 480 nm because of the conjugated DOX molecule. IONPs showed a high absorption peak at approximately 360–400 nm and maintained a high intensity in a scale range of up to 900 nm. In the case of only BRE, no significant peak was observed, except for a minor peak at 360–400 nm. DOX-BRE-IONPs showed a high intensity absorption peak in the 600–800 nm region, which is sufficient for photothermal therapy. Hence, the synthesized DOX-BRE-IONPs could be an excellent material for photothermal therapy.

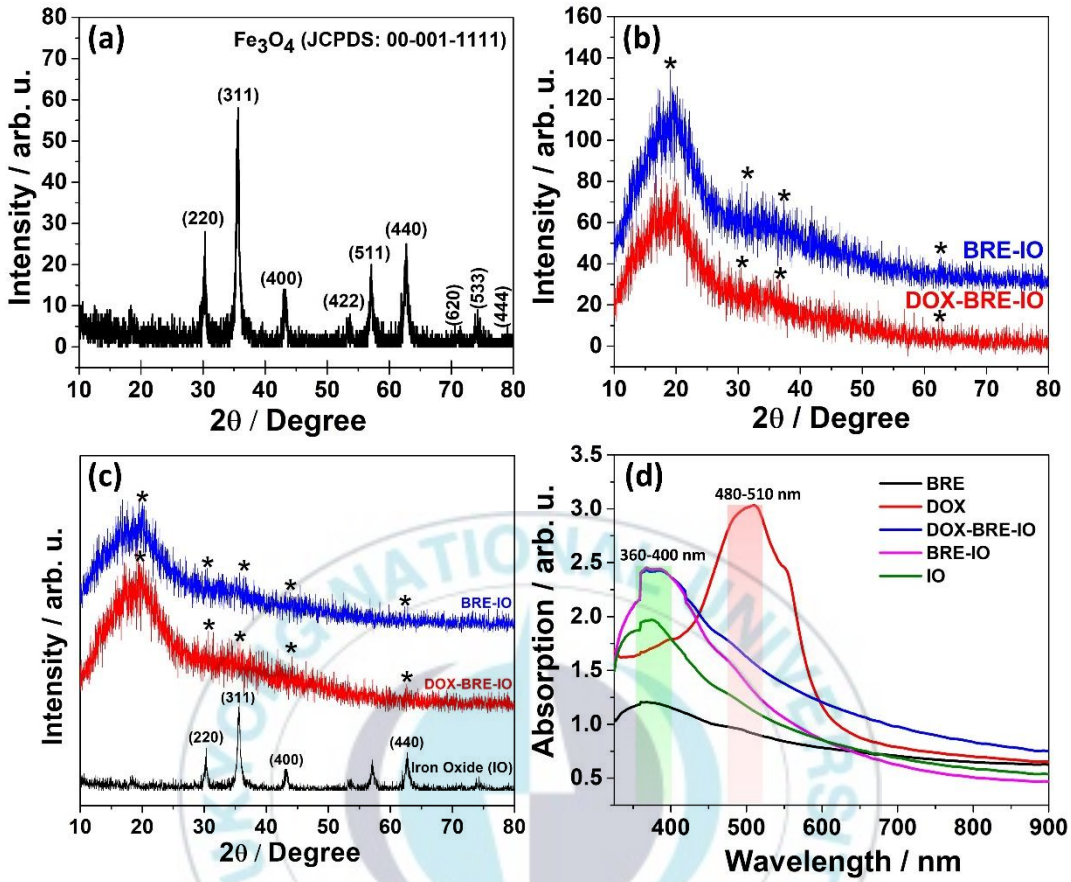

Figure 2: X-ray diffraction (XRD) analysis of (a) IONPs, (b) BRE-IONPs, DOX-BRE-IONPs and (c) comparing IONPs, BRE-IONPs, and DOX-BRE-IONPs. (d) UV-vis absorption spectra of IONPs, BRE, DOX, BRE-IONPs, and DOX-BRE-IONPs.

3. Fourier-transform infrared spectroscopy (FTIR) analysis

The FTIR spectra of the synthesized IONPs, BRE, BRE-IONPs, and DOX-BRE-IONPs are depicted in Figure 3a, b, c and d, respectively. Pristine magnetic IONPs showed a sharp band at ~626 cm^{-1}, which belongs to the Fe–O vibration for IO. The peaks observed at 1088 cm^{-1} is characteristic of the surface Fe–OH groups [32]. The fingerprint spectrum, which is characteristic of pure BRE, exhibited three peaks corresponding to the stretching of C–O. The wide peak monitored for the O–H stretching vibrations in the BRE spectra around 3266 cm^{-1}. The representative

peaks at 1651 cm^{-1} for –COO– unsymmetrical and 1402 cm^{-1} for –COO– symmetrical stretching vibrations, respectively. The absorption bands for pure BRE at 1158, 1011, 1653 and 1458 cm^{-1} shown in Figure. 3b and c were shifted to 1154, 997, 1658, and 1458 cm^{-1} for BRE-IONPs.

A broad band detected at ~3398 cm^{-1}, was attributed to O–H stretching, and another broad band at 2033 cm^{-1} was identified may be because of C–H stretching of BRE-IONPs. Peaks detected at 619 cm^{-1} and 574 cm^{-1} for BRE-IONPs due to the stretching vibrations of Fe-O bond which confirms the coating of BRE on the surface of IONPs, occurs via hydrogen bonding or coordination linkages [33, 34]. The band shift from 1651 cm^{-1} to 1658 cm^{-1} was observed for BRE-coated IONPs. A higher band shift from 1416 cm^{-1} to 1353 cm^{-1} noted for BRE-IONPs may be because of the hydrogen bonding between the hydrogen of the hydroxyl group in the BRE structure and the oxygen of IONPs [10]. After DOX loading, the peak at 1011 cm^{-1}, denoted the interaction of N–H scissoring in pure DOX that was diminished in the FTIR spectrum for DOX-BRE-IONPs. The attachment of DOX with BRE-IONPs, occurs via interaction between $–NH_2$ and –OH groups (for DOX molecule) with the –OH groups (for starch) through hydrogen bonding [10]. As shown in Fig. 2d, peaks at 1011–1156 cm^{-1} (C–O–C) and at 936 cm^{-1} (C–O) correspond to the present of DOX molecule.

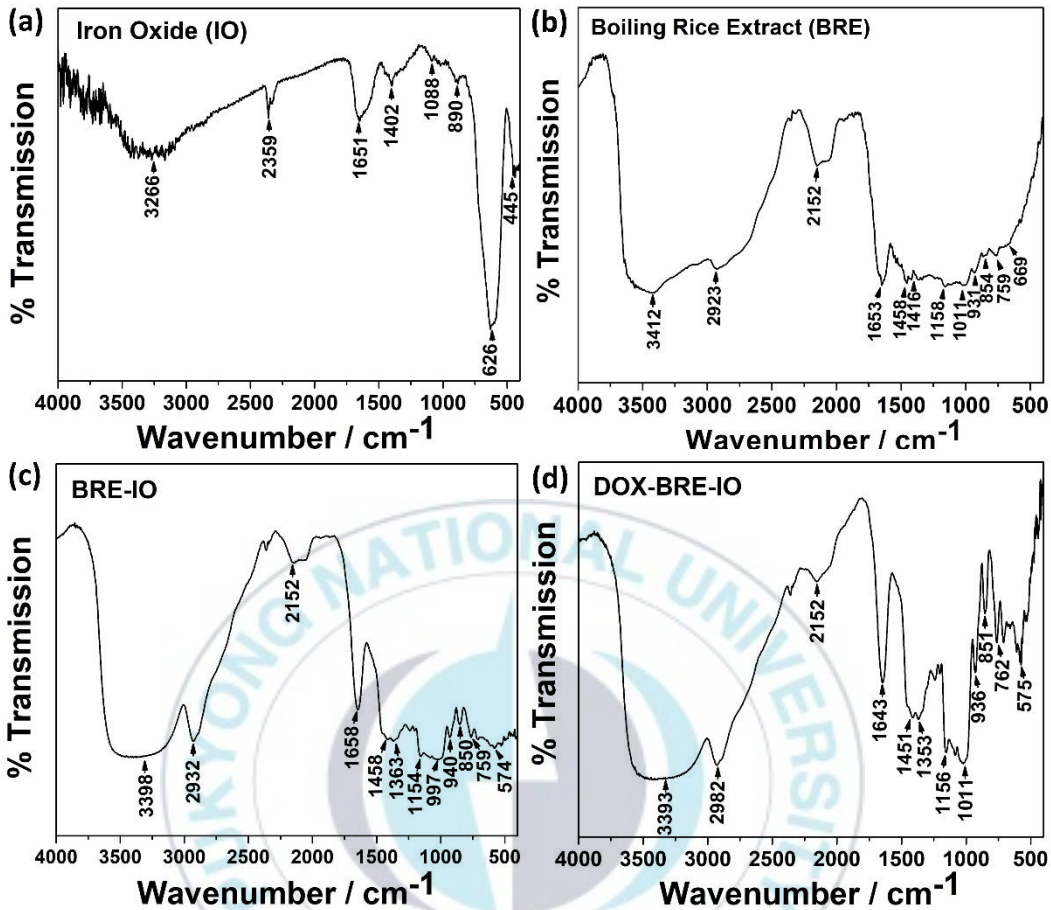

Figure 3: FT-IR characterization of (a) IONPs, (b) BRE, (c) BRE-IONPs, and (d) DOX-BRE-IONPs.

Table 1: FTIR Spectra analysis of IONPs, BRE, BRE-IONPs, and DOX-BRE-IONPs

Iron oxide	BRE	BRE-IONPs	DOX-BRE-IONPs	Functional groups
3266	2923-3412	2932-3398	2928-3393	O-H stretching vibration
-	2152	2152	2152	C-C stretching vibration

1651	1653	1658	1643	O-H stretch mode
-	1158-1458	1154-1458	1156-1451	C-O stretching vibration
890-1088	854-1011	850-997	851-1011	C-O stretching vibration
626	-	574-759	575-762	Fe-O stretching vibration

4. Micro Raman spectrometry analysis

The Raman spectrum of IONPs, BRE-IONPs, and DOX-BRE-IONPs was measured and is shown in Figure 4a and b. The positions of bands, modes, and functional groups for pristine IONPs, BRE-IONPs, and DOX-BRE-IONPs are summarized in Table 2. For IO, the ν1(FeO) band was very intense, similar to BRE-IONPs, and was associated with the Fe symmetric (ν1) stretching mode of the free tetrahedral Fe ion. This similar band was also recorded for BRE-IONPs [35]. The Raman spectra of synthesized IONPs are illustrated in Figure 4a, b. In this study, a 530 nm laser was used to excite the sample in the range of 220–2000 cm^{-1}. The recorded Raman spectra revealed sharp peaks at 1272 cm^{-1} because of ν3(FeO) vibration. The Raman spectra of BRE-IONPs and DOX-loaded BRE-IONPs revealed several distinct peaks. Most peaks are associated with the starch materials present in BRE. No significant differences were observed in BRE-IONPs and DOX-BRE-IONPs, except for the high intensity of the DOX-loaded material. The high intensity observed may be because of the fluorescence effect of DOX.

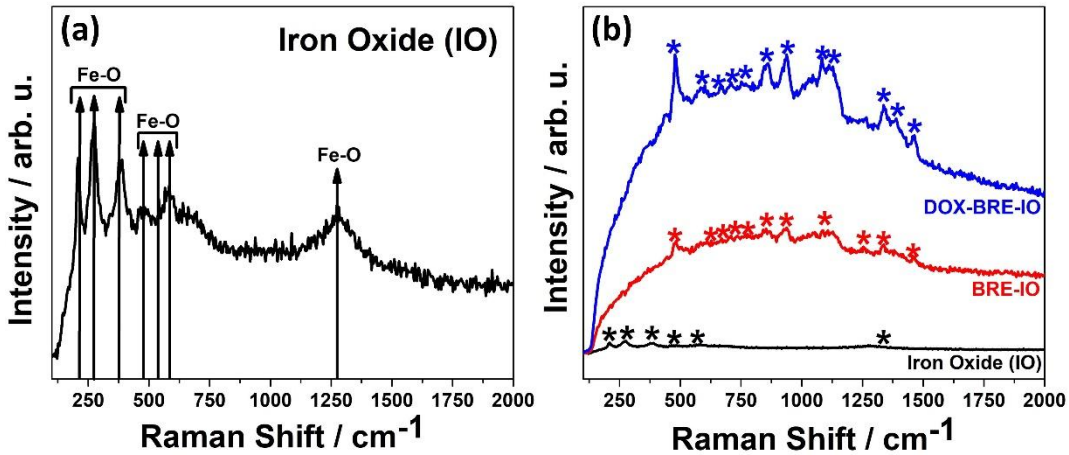

Figure 4: Raman spectra of (a) IONPs, (b) comparing Raman spectra of IONPs, BRE-IONPs, and DOX-BRE-IONPs.

Table 2: Raman spectra of IONPs, BRE-IONPs, and DOX-BRE-IONPs

Band (cm^{-1})	Assigned to	References
484	Skeletal modes of carbohydrate rings (δ(C-C-O))	[36, 37]
611	Unidentified	-
671-774	Unidentified	-
855	δ(CH_2, C(1)-H)), δ(C-O-H), C-C-H	[38, 39]
939	α-1,4-glycosidic linkage	[36, 38]
1087	δ(C-O-H) modes	[38]
1109	ν(C-O) δ(C-O-H) modes	[37-39]
1336-1377	δ(CH_2) scissoring	[38, 39]

5. Thermogravimetry-differential thermal (TG-DT) analysis

Thermogravimetry analysis of IONPs, BRE-IONPs, and DOX-BRE-IONPs was performed in a nitrogen-rich environment. The heating rate was controlled at 10 °C/min in room atmosphere. TG-DT analysis found that IO is thermally stable although the temperature was increased to 800 °C. From the TG curve (Figure 5a), a total weight loss of approximately 6% was estimated. Because of the evaporation of the coating materials, initial weight loss occurred at up to 280 °C for BRE-IONPs. While heating was increased to 500 °C, a major weight loss of up to 80% observed because of the presence of BRE. BRE-IONPs comprises a very low amount of IO, which causes a major weight loss that occurs when the temperature increases. Finally, no further weight loss was observed when the temperature was increased to 800 °C. Such a large difference was observed for BRE-IONPs and DOX-BRE-IONPs because of the loading of a very small quantity of DOX molecule.

In the differential thermal analysis study, we found three exothermic peaks at 203 °C, 269 °C, and 460 °C, respectively. The major exothermic peaks observed at 269 °C were due to the exothermic heat generation corresponding to the material's phase change [40]. The major exothermic peaks are observed at 349 °C and 500 °C depicted in Figure 5b. The major exothermic peaks observed at 349 °C were due to thermal instability and phase change. Two endothermic peaks were observed at 455 °C and 520 °C in Figure 5c, for DOX-BRE-IONPs. Two sharp exothermic peaks were observed at 356 °C and 498 °C, respectively in Figure 5c. Two endothermic peaks were observed at 434 °C and 536 °C. No such large difference was observed for BRE-IONPs and DOX-BRE-IONPs.

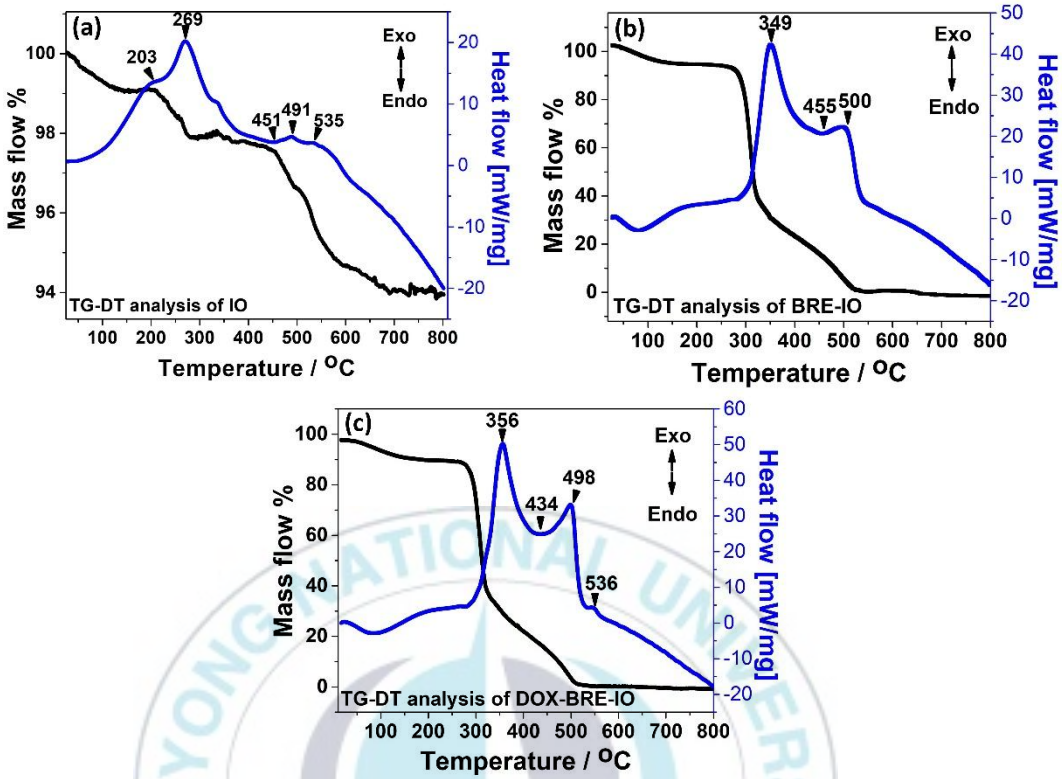

Figure 5: TG DT analysis of (a) IONPs, (b) BRE-IONPs, and (c) DOX-BRE-IONPs.

6. Field-emission-transmission electron microscope (FE-TEM) and Energy-dispersive X-ray spectroscopy (EDS) analyses

FE-TEM analysis was performed to determine the surface morphology of the synthesized IONPs and BRE-IONPs (Figure 6). The FE-TEM micrograph showed that the structure of IONPs was mostly spherical and well-dispersed, with an average nanometer size range [30]. Besides, BRE coating over IONPs appeared as a cluster, may be due to the interaction of the hydroxyl and carboxyl groups of BRE which present on adjacent to IONPs, as shown in Figure 6b, c.

EDS analysis confirmed the presence of Fe and O in IONPs (Figure 6d). Major EDS peaks for Fe were found, whereas, Si, P, K, Na, Cr, and O peaks were found

because of BRE (Figure 6e). BRE is mainly rice starch, that consists of many microelements, which were detected using EDS. As HCl-DOX was used to prepare DOX-BRE-IONPs, EDS analysis (Figure 5e) showed the presence of "Cl" in the DOX-BRE-IONPs complex structure. The average particle size of IONPs relies within 86 ± 3.6 nm range (Figure 6a). In Figure 6b, the successful coating of BRE on IONPs is observed, whereas, in Figure 6c, DOX loaded BRE-IONPs were shown. The DOX-BRE-IONPs further used for photothermal therapy to treat cancer cells. There are no morphological changes observed post PTT experiment (Figure 7).

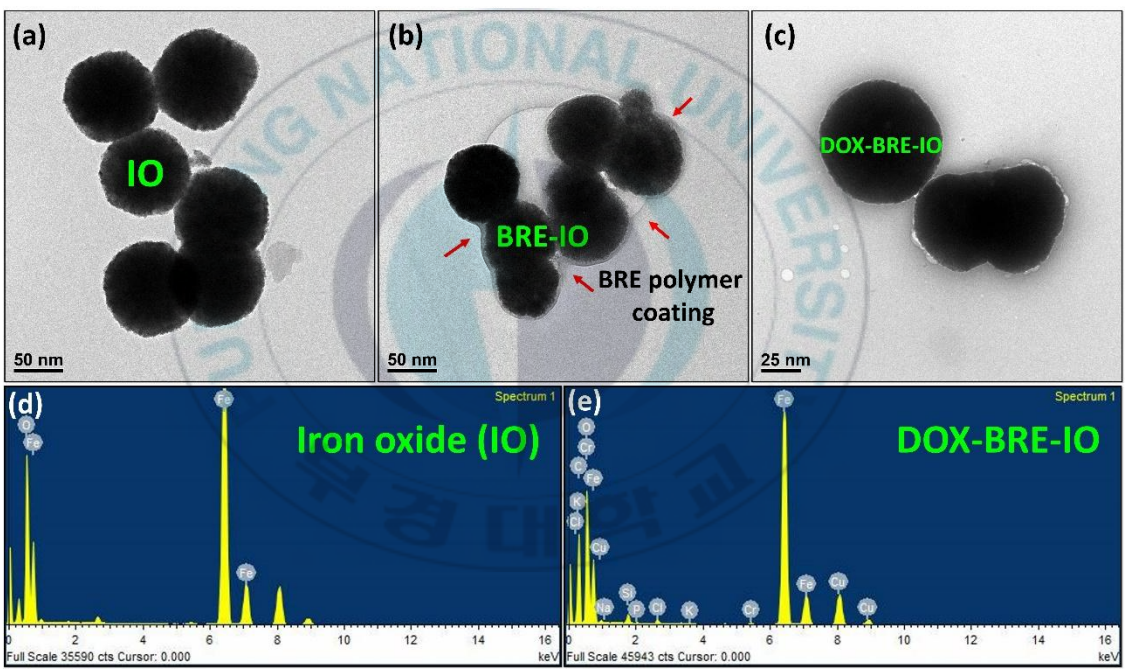

Figure 6: Field emission transmission electron microscopy (FE-TEM) analysis of (a) IONPs, (b) BRE-IONPs, (c) DOX-BRE-IONPs, (d) EDS analysis of IONPs and (e) DOX-BRE-IONPs.

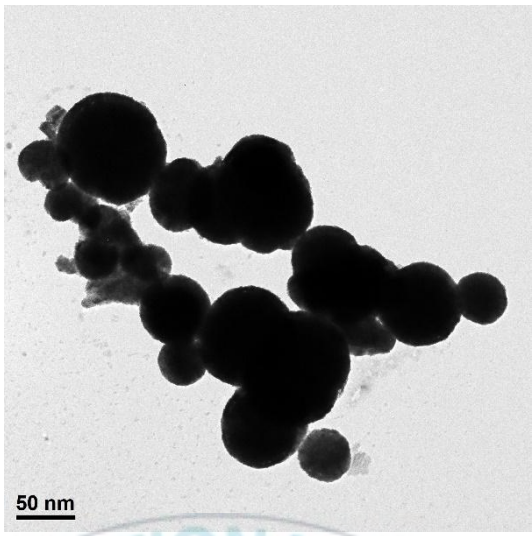

Figure 7: The FE-TEM image of DOX-BRE-IONPs post-photothermal treatment.

7. Zeta-potential study

Zeta-potential measurements were performed in different pH (4.5, 7.2, 9.0) conditions to investigate the surface charges and the stability of the BRE, BRE-IO, and DOX-BRE-IONPs (Figure 8a). Zeta potential measurements were used to reveal the electrostatic interaction between the metal oxide (iron oxide), starch, and drug (DOX) molecules. All BRE, BRE-IO, and DOX-BRE-IONPs showed negatively charged surface and became more negative when the pH was increased. The high absolute zeta potential values could increase electrostatic repulsion among nanoparticles to prevent aggregation. The surface charges of BRE were -2.1mV (at pH 4.5), -3.4 mV (at pH 7.2), and -8.4 mV (at pH 9.0), respectively. The zeta potential values for BRE-IONPs were measured as -1.7mV (at pH 4.5), -5.4 mV (at pH 7.2), and -7.8 mV (at pH 9.0), respectively. A high negative zeta potential of BRE-IONPs suggests the presence of numerous carboxyl groups which makes a good colloidal stability [41]. The BRE-IONPs were stable in size across the entire pH range and were ideal for the encapsulation and transportation of DOX molecules.

The zeta potential values for DOX-BRE-IONPs was found to be -2.1 mV (at pH 4.5), -4.2 mV (at pH 7.2), and -7.2 mV (at pH 9.0), respectively. The decrease in absolute value of zeta potential in case of DOX-BRE-IONPs are may be due to the neutralization of surface charge of BRE molecules [42]. From this study, the DOX-BRE-IONPs were found in the entire pH range with high colloidal stable condition and no precipitation or aggregation was observed.

8. Vibrating sample magnetometer

The magnetic saturation experiment was performed on IONPs and DOX-BRE-IONPs (Figure 8b). IONPs produced a strong magnetic saturation behavior of ~70.65 emu/g. For DOX-BRE-IONPs, a magnetic saturation of ~48.69 emu/g, which is less than that of IONPs because of the BRE-coating effects, was observed. The magnetic saturation for DOX-BRE-IONPs is sufficient to generate an external force to target the nanoparticles in the affected tissues. The synthesized IONPs and BRE-IONPs showed superparamagnetic characteristics, with less coercivity and remnant magnetization. BRE did not show any hysteresis loop because of nonmagnetic properties.

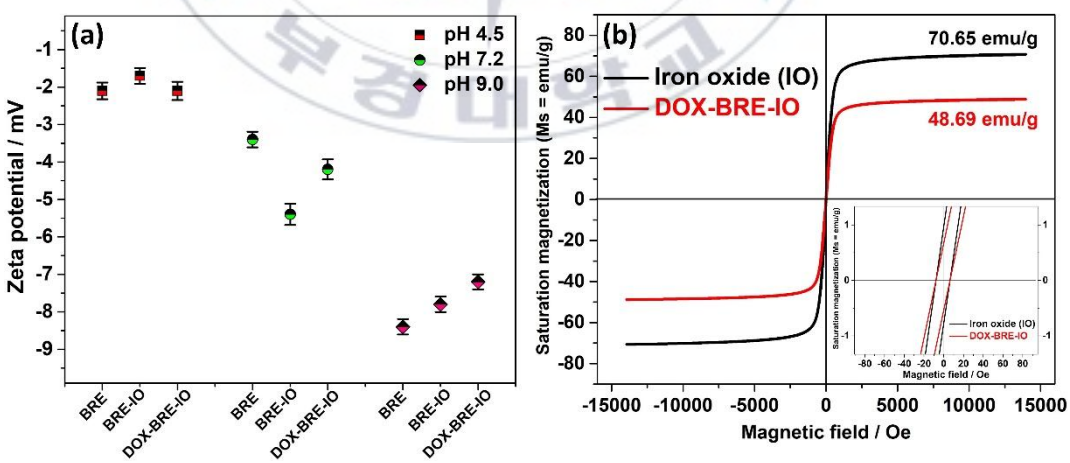

Figure 8: (a) Zeta potential study of BRE, BRE-IONPs, DOX-BRE-IONPs at different pH conditions (pH 4.5, 7.2, 9.0). (b) Magnetization curve of IONPs and DOX-BRE-IONPs (inset corresponds to a low-field region of IONPs and DOX-

BRE-IONPs magnetic saturation curve to identify the coercivity and remanent magnetization).

9. Kinetics of DOX loading and release

The capacity of the carrier to efficiently release the drug at the desired site is an important feature of any delivery system. The amount of drug or the degree of adsorption of the adsorbing materials depends on their surface charge, surface area, pore size, and pore volume. To estimate the model drug (DOX) interactions with synthesized DOX-BRE-IONPs, drug loading and releasing kinetics were studied. The prepared DOX solution was used as a stock with which the nanoparticles were mixed, and after 24 h incubation, the UV-vis spectra were measured to estimate DOX loading amount on nanoparticle surface. The initial and final DOX concentration after the incubation of nanoparticles was calculated for effective DOX loading. The loaded DOX was actively adsorbed on BRE-IONPs. The DOX-loaded BRE-IONPs were air-dried in an oven and stored for future use. The quantity of the loaded drug was calculated using the following equation.

$$\text{Loading efficiency (\%)} = \frac{Total\ amount\ of\ drug - Total\ amount\ of\ free\ drug}{Total\ amount\ of\ drug} \times 100\ (\%)$$

The calculated amount of the loaded DOX on BRE-IONPs was ~78 %, which is sufficient for a drug carrier. DOX-loaded BRE-IONPs were further studied for drug release in different pH (9.0, 7.2, 4.5) environment (Figure 9). The release pattern of DOX molecules from the system varied with different pH values. The maximum drug release was obtained in the acidic (pH 4.5) environment, which was ~46% of the loaded drug. For neutral pH 7.2, the least amount of drug release was observed, which was ~14% of the loaded drug. For the basic environment, the maximum

amount of loaded drug released was ~20 %. For the first 12 h, the release pattern observed was considered as the burst release, whereas a sustainable prolonged release pattern was observed after 12 h. In case of the acidic (pH 4.5) environment, a well-controlled sustainable drug release pattern was calculated up to 96 h. All drug release experiments were performed using UV-vis spectroscopy. The following equation was used to calculate the cumulative drug release.

$$\text{Cumulative drug release (\%)} = \frac{concentration\ of\ drug\ released}{concentration\ of\ total\ drug} \times 100\ (\%)$$

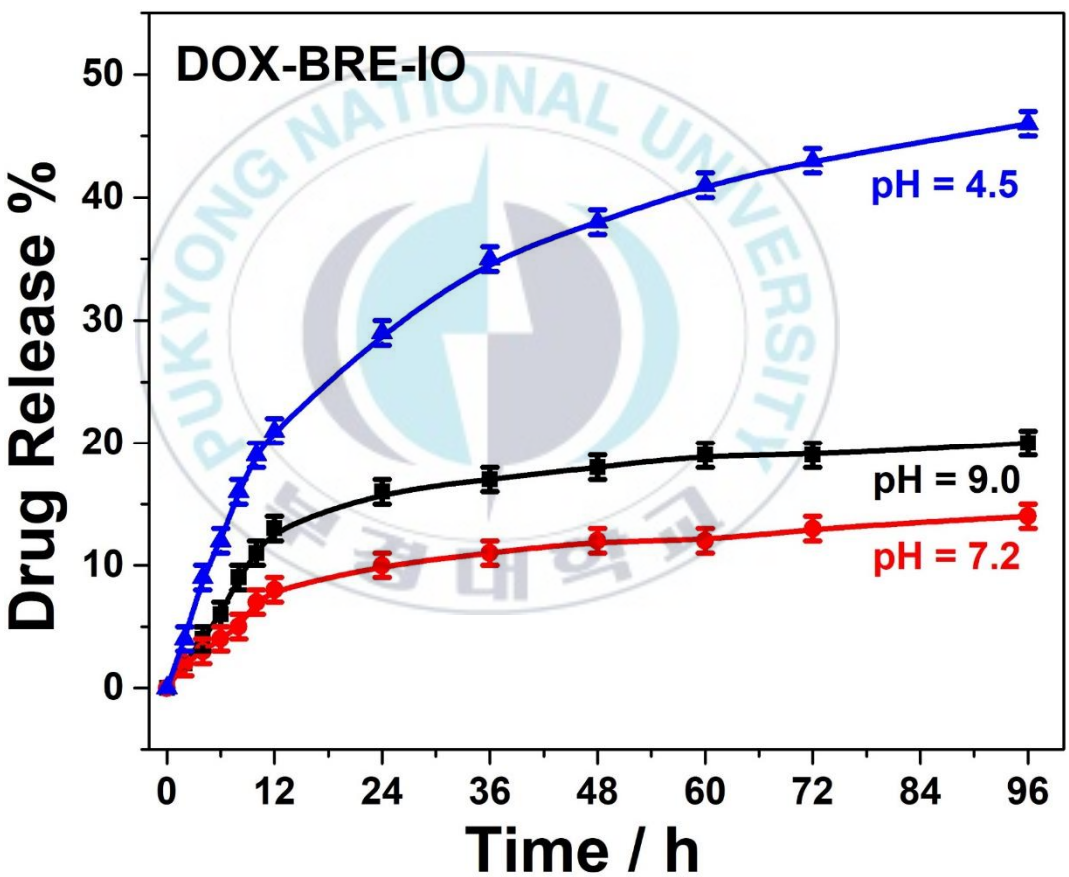

Figure 9: Drug (DOX) release kinetics of BRE-IONPs at different pH and time intervals.

The release pattern of the loaded DOX was well correlated with the Higuchi model. The Higuchi model is associated with the calculation of the simultaneous dissolution and diffusion of the drug-releasing system. To explain BRE-IONPs drug release kinetics, the "Higuchi model" is represented with the following equation [43, 44].

$$Q = A\sqrt{D(2C_0 - C_s)C_s \times t}$$

where Q is the amount of drug (DOX) released in time t per unit area, C_0 is the initial concentration of DOX, C_s is the DOX solubility in the media, and D is the diffusivity of DOX molecules in the matrix substance.

10. Biological evaluations

10.1 Cell viability

Cell viability was evaluated using toxicity determination experiments where the nanoparticles were incubated with cells in different conditions. To study the toxicity effect of synthesized IONPs, BRE-IONPs and DOX-BRE-IONPs, the MTT assay using MG-63 osteoblast cell lines (Figure 10a) was performed. The nanoparticles were incubated with MG-63 cells at different concentrations (50, 100, 150, 200, and 250 μg/mL) for 24 h. The control was treated without nanoparticles. The MTT assay revealed the nontoxic behavior of BRE-IONPs even at high concentrations of 250 μg/mL. IONPs showed a mild toxicity at a lower concentration of 50 μg/mL, whereas at a higher concentration (250 μg/mL), it showed a greater toxicity. IONPs revealed ~60% cell viability, whereas DOX-BRE-IONPs showed a highly toxic effect. The toxicity level of DOX-BRE-IONPs increased with increasing concentration. A nanoparticle concentration of 250 μg/mL showed approximately 30% cell viability, which confirms the high level of toxicity due to DOX. BRE-IONPs toxicity by itself is lower because of its biocompatible coating. BRE coating helped load the DOX molecule on the nanostructured materials surface.

The MTT study was extended using different time intervals to determine whether any toxic effect is generated because of long-term incubation (Figure 10b). The results revealed that BRE is an excellent biocompatible material when used as a coating material over IONPs because no toxic effect was observed. IONPs showed a toxic effect with different concentrations as well as with different incubation times. IONPs 200 µg/mL showed ~60% cell viability after 24 h incubation, and the toxicity level increased by up to ~50% within 48 h. After 72 h incubation, ~45% of the cells were viable. For DOX-BRE-IONPs, the toxicity level was extremely high. After 24 h of incubation, ~60% cells died, whereas ~38% and ~35% cell viability was achieved after 48 h and 72 h incubation, respectively. The time-dependent cell viability study showed the toxic effect of IONPs and DOX molecules, whereas controls and BRE-coated IONPs revealed a nontoxic effect.

10.2 AO/PI fluorescence study

AO/PI live/dead cell assay was performed to determine the cell viability (Figure 10c). In this assay, live cells emit green fluorescence, whereas dead cells emit red fluorescence. The controls showed almost all green fluorescence; whereas ~65% green fluorescence for IONPs incubated for 24 h, ~58% for 48 h, and ~55% for 72 h respectively. BRE-IONPs treated MG-63 cell lines showed very less quantity of red fluorescence, which confirms the nontoxic effect of BRE-IONPs. DOX-BRE-IONPs showed a lethal toxic effect, and consequently, the cells emitted mostly red fluorescence. Hence, IONPs revealed the toxic effect to cell lines, whereas BRE-IONPs show less/no toxicity. The same BRE-IONPs when loaded with DOX show lethal toxicity to MG-63 cells. This study is aimed to treat cancer by means of combination of chemotherapeutic and photothermal study guided by PAI. The entire in vitro study was performed with MG-63 osteoblast cell lines.

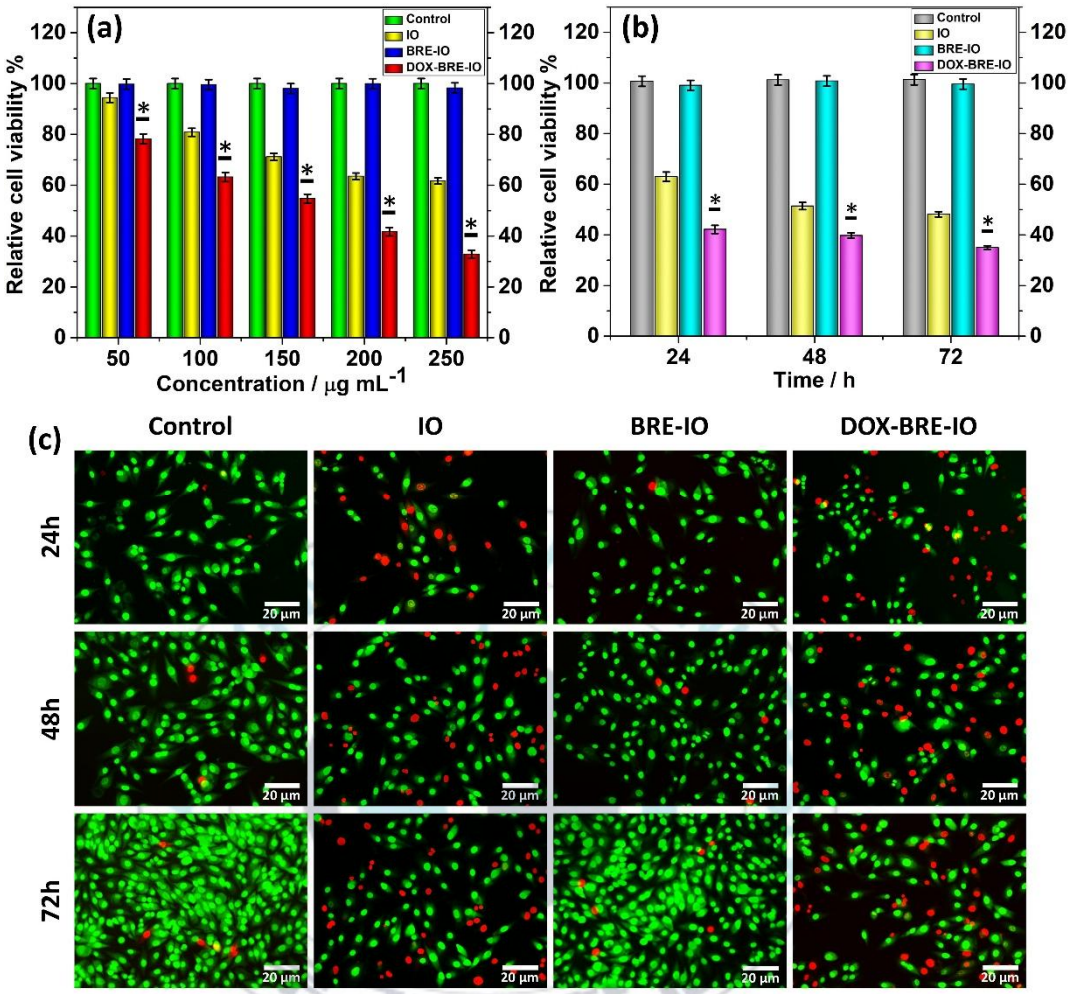

Figure 10: In vitro biocompatibility and cell cytotoxicity study (MTT assay) of IONPs, BRE-IONPs, DOX-BRE-IONPs at (a) different concentrations of 50, 100, 150, 200, and 250 μg/mL (All results were expressed as mean standard deviation (S.D). (n = 5, *significant $p < 0.05$ vs control as statistically significant). (b) Different time interval of 24, 48, and 72 on MG-63 osteoblast cell lines (All results were expressed as mean standard deviation (S.D). (n = 5, *significant $p < 0.05$ vs control as statistically significant). (c) AO/PI fluorescence study after 24, 48, 72h incubation with MG-63 osteoblast cell lines.

11. Photothermal performance of IONPs, BRE-IONPs and DOX-BRE-IONPs

11.1 Photothermal behavior of IONPs, BRE-IONPs and DOX-BRE-IONPs

The synthesized IONPs, BRE-IONPs and DOX-BRE-IONPs were studied for photothermal therapy. Figure 11a, shows the graph for temperature changes with variable times after irradiating the samples with 1.0 W/cm^2 NIR laser. IONPs solution temperature was increased up to 70.5 °C after 5 min; whereas BRE-IONPs and DOX-BRE-IONPs solution increased the temperature up to 59.8 °C and 59.2 °C respectively in 5 min, which is sufficient to kill cancer cells using PTT. For only PBS solution (without any nanoparticles) no temperature elevation observed. From the above results, IONPs, BRE-IONPs, and DOX-BRE-IONPs revealed their potential as a promising photothermal agent for PTT. The photothermal stability is an important property of nanoparticles used for PTT purposes. As depicted in Figure 11b, after five heating and cooling cycles under the 1.0 W/cm^2 808-nm NIR laser irradiation, the material was highly stable, and generated heat of up to 60 °C in 5 min and cooled down to 23 °C after 15 min. For each cycle, the thermal curve of the DOX-BRE-IONPs solution was stable. The NIR thermographic images of PBS, IONPs, BRE-IONPs, and DOX-BRE-IONPs solution are represented in Figure 11c. This present study suggested that DOX-BRE-IONPs are good photothermal agents with high stability during long-term laser irradiation.

11.2 Cell-killing effect of IONPs, BRE-IONPs and DOX-BRE-IONPs with laser exposure

IONPs, BRE-IONPs and DOX-BRE-IONPs were analysed to quantify their photothermal destruction capability over MG-63 cells using the MTT assay (Figure 12a). MTT results showed without nanoparticles there is no cell death. The IONPs treated cells after laser irradiation shows ~18% of viable cells, whereas ~22%

healthy cells were observed for BRE-IONPs and laser treated cell lines. The lethal effect of DOX-BRE-IONPs treatment with laser irradiation shows only ~5 % live cells. Due to the effect of the combination of DOX and PTT, most cells died. This study confirms the efficiency of DOX-BRE-IONPs accompanied with NIR laser as a photothermal agent in PTT to kill cancer cells. After laser irradiation, AO/PI fluorescent images were performed to investigate the *in vitro* PTT effect of IONPs, BRE-IONPs, and DOX-BRE-IONPs (Figure 12b). AO/PI fluorescent staining was performed to differentiate the live and dead cells. AO enters viable cells and emits green fluorescence, whereas PI enters through damaged cell membranes and emitting red fluorescence. The control group (Group I) showed a high number of green fluorescence because of live cells. All the remaining three groups showed more dead cells because of the photothermal heating of IONPs. In Group IV, the additional lethal effect of DOX along with the NIR laser generates photothermal effects which causes maximum cell death.

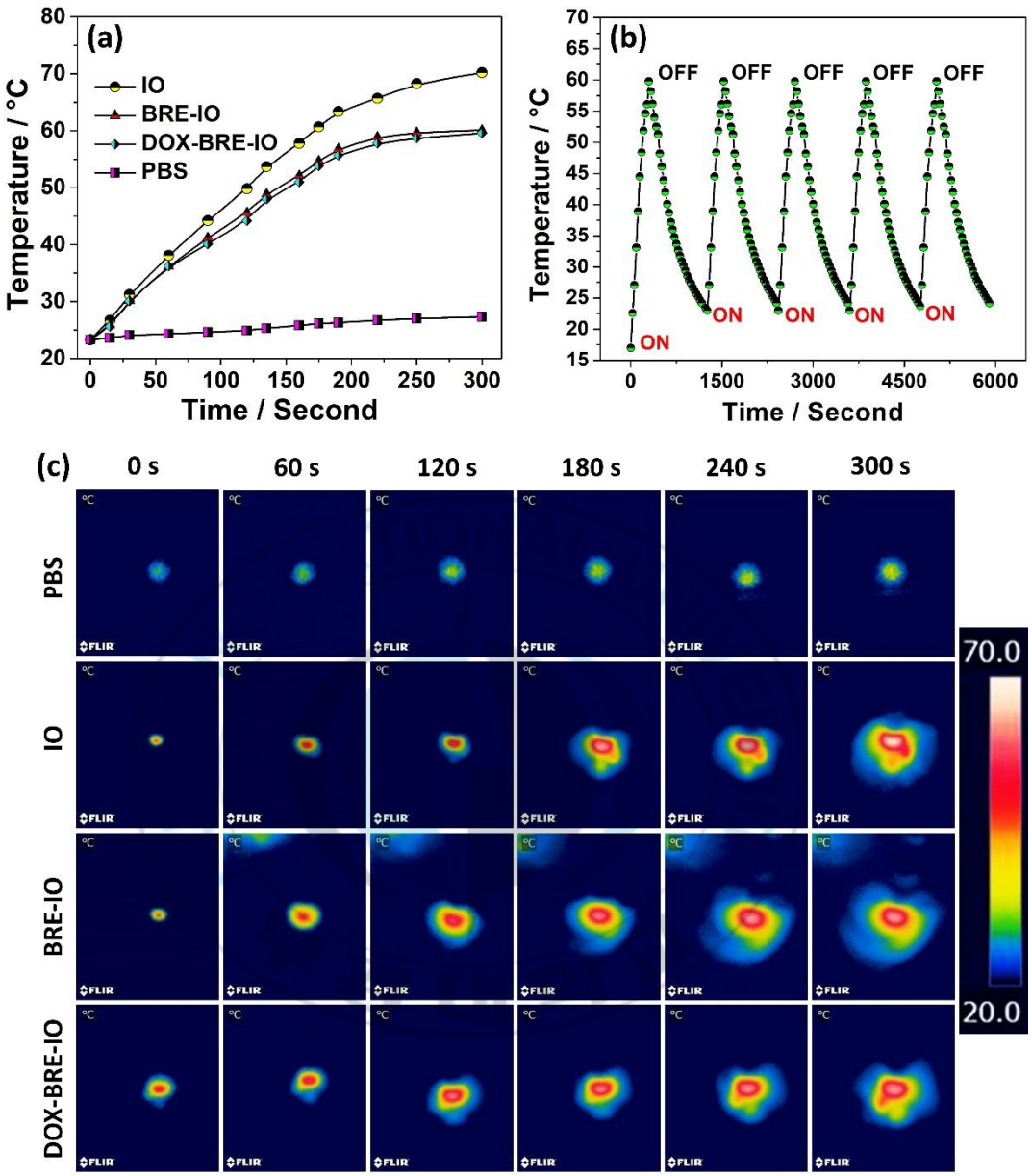

Figure 11: Thermal properties of IONPs, BRE-IONPs, and DOX-BRE-IONPs. (a) Heating curve of IONPs, BRE-IONPs, and DOX-BRE-IONPs under irradiation (808 nm laser, 1.0 W/cm^2, 5 min). (b) Thermal stability of DOX-BRE-IONPs (200 μg/mL, 808 nm laser, 1.0 W/cm^2, 5 min). (c) The NIR thermographic images of PBS, IONPs, BRE-IONPs, and DOX-BRE-IONPs solution under irradiation (200 μg/mL, 808 nm laser, 1.0 W/cm^2, 5 min).

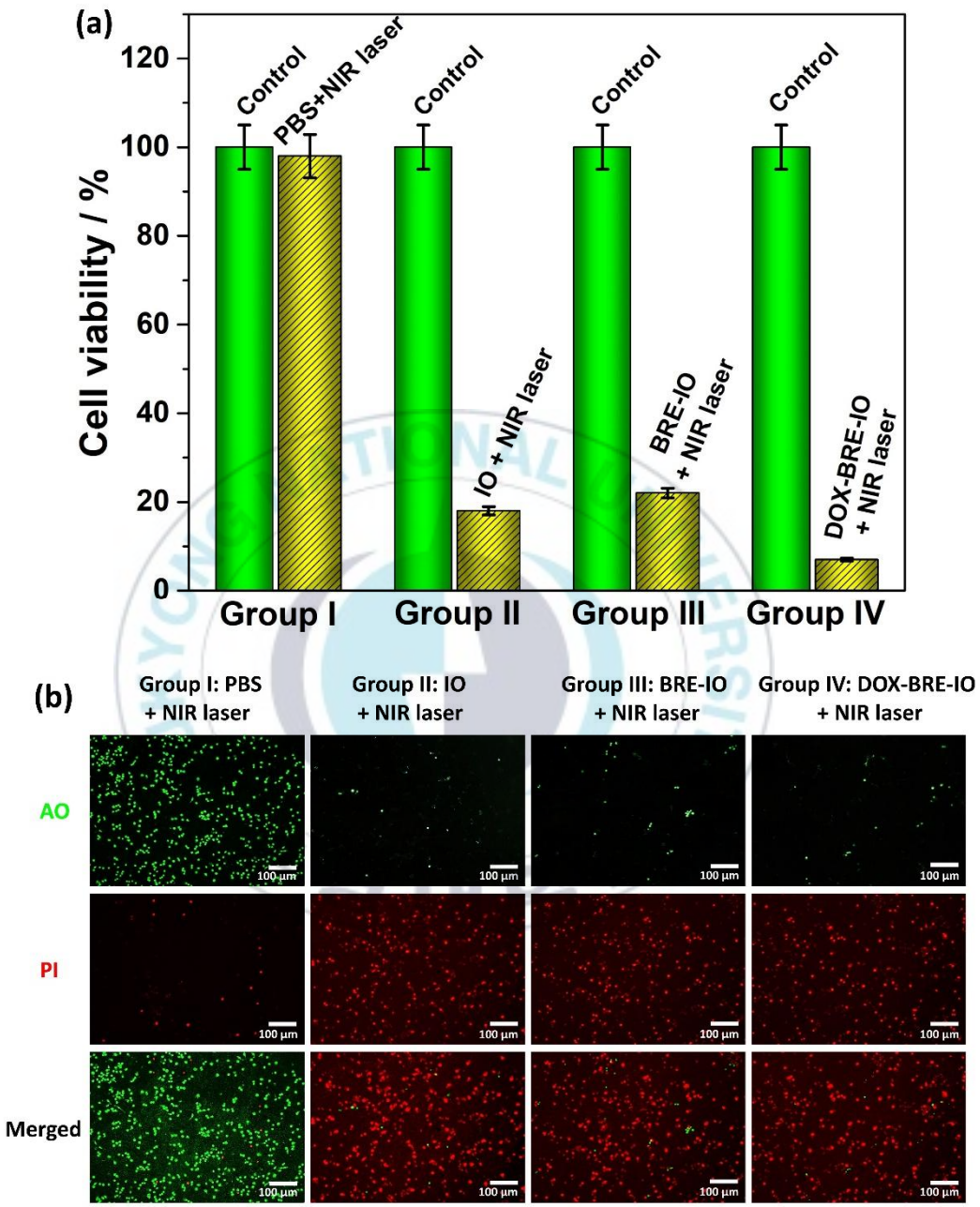

Figure 12: (a). The cell viability of MG-63 cells treated with PBS, IONPs, BRE-IONPs and DOX-BRE-IONPs under irradiation (200 μg/mL, 808 nm laser, 1.0 W/cm^2, 5 min). (b) AO and PI staining of MG-63 cells treated with PBS,

IONPs, BRE-IONPs and DOX-BRE-IONPs plus NIR laser (200 μg/mL, 1.0 W/cm^2, 5 min).

12. Photoacoustic performance of DOX-BRE-IONPs

PAI is an emerging noninvasive imaging technique for diagnosis of diseased or affected tissues. In this study, an indigenously developed PAI system (Ohlabs corp. Busan, Republic of Korea) used to acquire the PA images of MG-63 cells treated with synthesized nanoparticles (Figure 13 and Figure 14a). For PA imaging, MG-63 cell lines were treated with different concentrations (25-400 μg/mL) of DOX-BRE-IONPs. The control tube was filled with DI water only (without nanoparticles). The PTFE tubes that contained MG-63 cells treated with a high concentration (400 μg/mL) of DOX-BRE-IONPs showed strong PA signals with increasing magnitude, whereas the control tube did not show any PA signals (Figure 14b). PAI signals got noticeably weaker with decreasing concentrations of nanoparticles. For 25 μg/mL nanoparticles, the signal was very poor. The recommended 200 μg/mL DOX-BRE-IONPs concentration could be useful for biomedical imaging purposes with safe and strong signal.

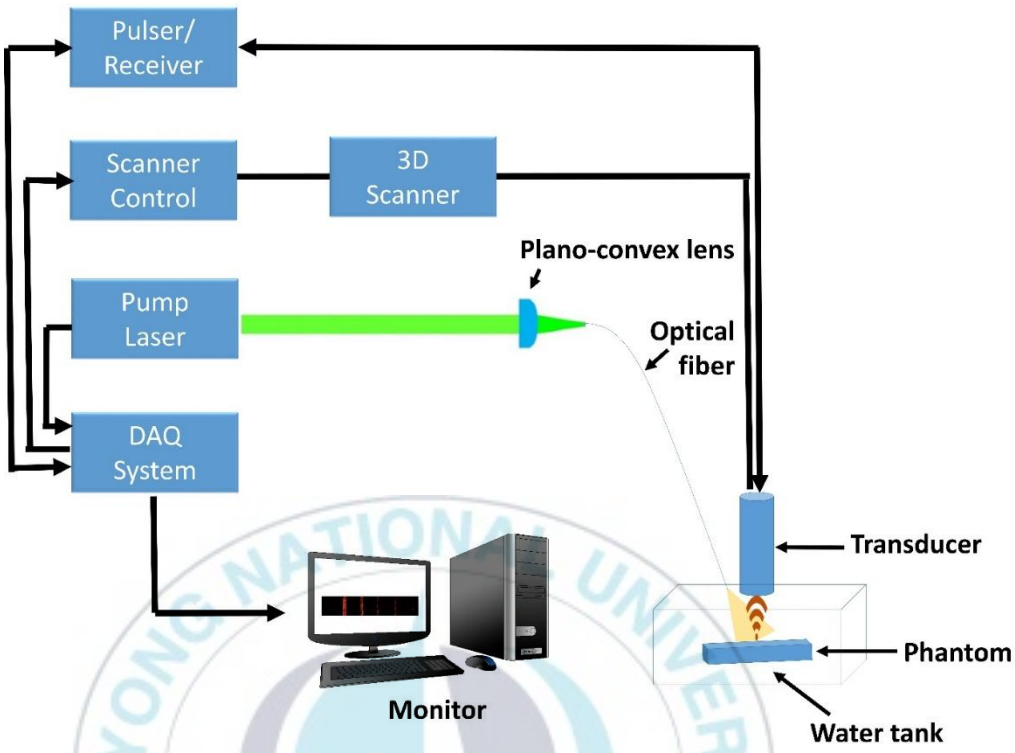

Figure 13: Experimental setup of PAI system.

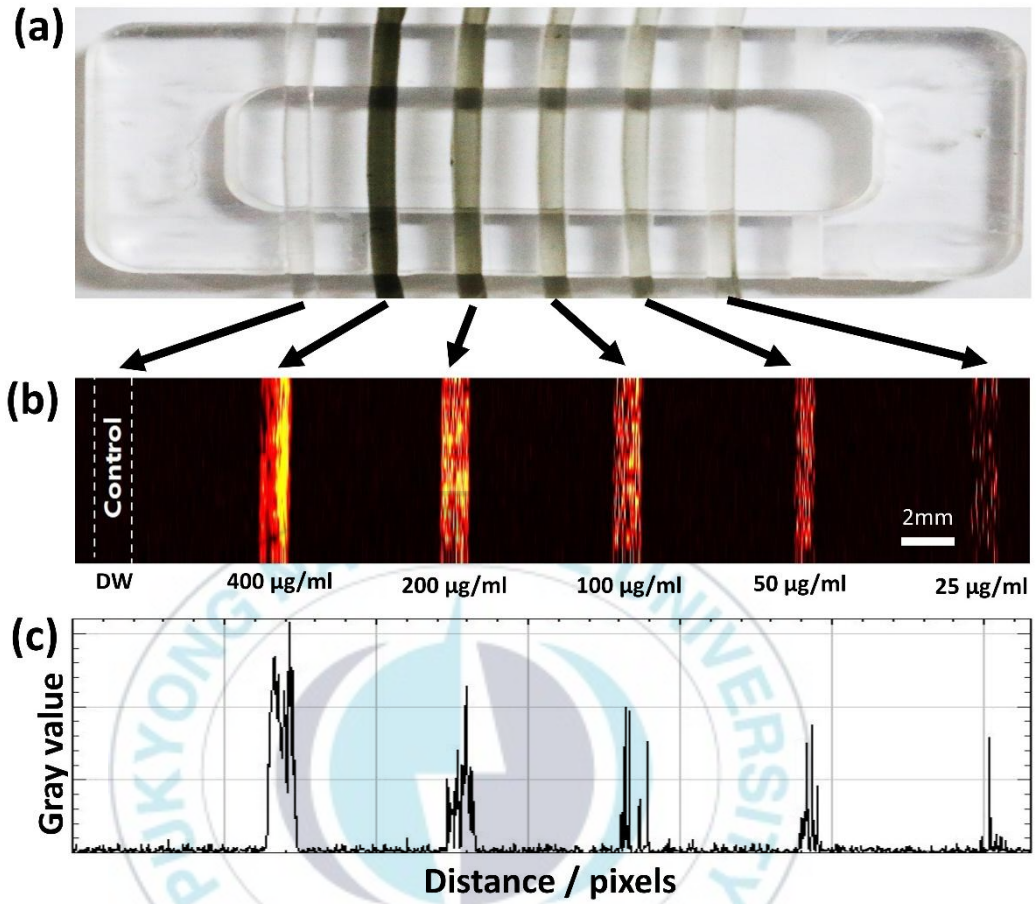

Figure 14: PAI experiment. (a) The PTFE tubes in a customized sample holder containing the DOX-BRE-IONPs with various concentrations. (b) The corresponding PA images. (c) The corresponding PAI amplitude profile.

Chapter 4. Discussion and conclusion

This study reports a successful solvothermal synthetic route for IONPs. The synthesized nanoparticles were further coated with non-toxic rice starch BRE, which results enhanced biocompatibility. BRE-IONPs was synthesized for NIR laser-triggered drug release in combination with chemo-photothermal therapy under the guidance of PAI. The characterization study confirms the elemental composition of Fe and O for IO spherical nanoparticles, with an average size of 86 ± 3.6 nm. The IONPs exhibited strong magnetic saturation behavior of ~70.65 emu/g. No apparent cytotoxic effects were observed at various BRE-IONPs concentrations. Thus, BRE could be useful as a promising biomaterial due to its availability as a raw material from an ecological and low-cost source with greater biocompatibility. The in vitro MTT assay of DOX-BRE-IONPs showed enhanced cytotoxic effect with greater drug uptake potential, which established the role of BRE-IONPs as an efficient drug carrier agent. The synthesized BRE-IONPs revealed its potential drug carrier capabilities with ~78% loaded DOX molecules. The pH dependent DOX releasing property reveals ~46% DOX release capability at acidic environment (pH 4.5) specifically targeting cancer cells. The PA imaging study successfully captured the DOX-BRE-IONPs engulfed by MG-63 cells. It is important to mention that DOX-BRE-IONPs could act as a promising contrast agent to enhance the PA signal, which is helpful for more precise imaging guidance for photothermal therapy. In vitro investigation demonstrated the tuned toxicity effect of BRE-IONPs in killing cancer cells when exposed to 808 nm NIR laser. The photothermal heat conversion efficiency is ~29.73% which is similar to those of classic photothermal agents including gold and silver. The properties of BRE-IONPs opens a new paradigm for multifunctional imaging-guided photothermal therapy with a great potential for cancer treatment.

References

[1] M.K.D. Manshadi, M. Saadat, M. Mohammadi, M. Shamsi, M. Dejam, R. Kamali, A. Sanati-Nezhad, Delivery of magnetic micro/nanoparticles and magnetic-based drug/cargo into arterial flow for targeted therapy, Drug Deliv. 25(1) (2018) 1963-1973.

[2] V. Hubert, C. Dumot, E. Ong, C. Amaz, E. Canet-Soulas, F. Chauveau, M. Wiart, MRI coupled with clinically-applicable iron oxide nanoparticles reveals choroid plexus involvement in a murine model of neuroinflammation, Sci Rep. 9(1) (2019) 1-9.

[3] J. Estelrich, M.A. Busquets, Iron Oxide Nanoparticles in Photothermal Therapy, Molecules 23(7) (2018).

[4] J.D. Rybka, Radiosensitizing properties of magnetic hyperthermia mediated by superparamagnetic iron oxide nanoparticles (SPIONs) on human cutaneous melanoma cell lines, Rep Pract Oncol Radiother. 24(2) (2019) 152-157.

[5] S.M. Dadfar, K. Roemhild, N.I. Drude, S. von Stillfried, R. Knüchel, F. Kiessling, T. Lammers, Iron oxide nanoparticles: Diagnostic, therapeutic and theranostic applications, Adv. Drug Deliv. Rev. 138 (2019) 302-325.

[6] G. Prabha, V. Raj, Preparation and characterization of polymer nanocomposites coated magnetic nanoparticles for drug delivery applications, J. Magn. Magn. Mater. 408 (2016) 26-34.

[7] S. Mondal, P. Manivasagan, S. Bharathiraja, M.S. Moorthy, H.H. Kim, H. Seo, K.D. Lee, J. Oh, Magnetic hydroxyapatite: a promising multifunctional platform for nanomedicine application, Int J Nanomedicine. 12 (2017) 8389.

[8] R.M. Cornell, U. Schwertmann, The iron oxides: structure, properties, reactions, occurrences and uses, John Wiley & Sons 2003.

[9] S. Laurent, A.A. Saei, S. Behzadi, A. Panahifar, M. Mahmoudi, Superparamagnetic iron oxide nanoparticles for delivery of therapeutic agents: opportunities and challenges, Expert Opin Drug Deliv. 11(9) (2014) 1449-1470.

[10] S. Kayal, R.V. Ramanujan, Anti-cancer drug loaded iron–gold core–shell nanoparticles (Fe@ Au) for magnetic drug targeting, J. Nanosci. Nanotechnol. 10(9) (2010) 5527-5539.

[11] S. Likhitkar, A. Bajpai, Magnetically controlled release of cisplatin from superparamagnetic starch nanoparticles, Carbohydr. Polym. 87(1) (2012) 300-308.

[12] M.K. Yu, Y.Y. Jeong, J. Park, S. Park, J.W. Kim, J.J. Min, K. Kim, S. Jon, Drug□loaded superparamagnetic iron oxide nanoparticles for combined cancer imaging and therapy in vivo, Angew Chem Int Ed. 47(29) (2008) 5362-5365.

[13] P.M. Khaniabadi, D. Shahbazi-Gahrouei, M.S. Jaafar, A.M.S.A. Majid, B.M. Khaniabadi, S. Shahbazi-Gahrouei, Magnetic iron oxide nanoparticles as T2 MR imaging contrast agent for detection of breast cancer (MCF-7) cell, Avicenna J. Med. Biotechnol. 9(4) (2017) 181.

[14] P. Manivasagan, S.W. Jun, G. Hoang, S. Mondal, H. Kim, V.H.M. Doan, J. Kim, C.-S. Kim, J. Oh, Anti-EGFR antibody conjugated thiol chitosan-layered gold nanoshells for dual-modal imaging-guided cancer combination therapy, J Control Release 311 (2019) 26-42.

[15] C. Tassa, S.Y. Shaw, R. Weissleder, Dextran-coated iron oxide nanoparticles: a versatile platform for targeted molecular imaging, molecular diagnostics, and therapy, Acc. Chem. Res. 44(10) (2011) 842-852.

[16] S. Kayal, R. Ramanujan, Doxorubicin loaded PVA coated iron oxide nanoparticles for targeted drug delivery, Mater. Sci. Eng. C. 30(3) (2010) 484-490.

[17] H. Elkhenany, M. Abd Elkodous, N.I. Ghoneim, T.A. Ahmed, S.M. Ahmed, I.K. Mohamed, N. El-Badri, Comparison of different uncoated and starch-coated superparamagnetic iron oxide nanoparticles: implications for stem cell tracking, Int. J. Biol. Macromol. 143 (2020) 763-774.

[18] N.S. Elbialy, N. Mohamed, Alginate-coated caseinate nanoparticles for doxorubicin delivery: Preparation, characterisation, and in vivo assessment, Int. J. Biol. Macromol. (2020).

[19] N.H. Moghadam, S. Salehzadeh, J. Rakhtshah, A.H. Moghadam, H. Tanzadehpanah, M. Saidijam, Preparation of a highly stable drug carrier by efficient immobilization of human serum albumin (HSA) on drug-loaded magnetic iron oxide nanoparticles, Int. J. Biol. Macromol. 125 (2019) 931-940.

[20] S. Mondal, G. Hoang, P. Manivasagan, M.S. Moorthy, T.T.V. Phan, H.H. Kim, T.P. Nguyen, J. Oh, Rapid microwave-assisted synthesis of gold loaded hydroxyapatite collagen nano-bio materials for drug delivery and tissue engineering application, Ceram. Int. 45(3) (2019) 2977-2988.

[21] P. Tartaj, C.J. Serna, Synthesis of monodisperse superparamagnetic Fe/silica nanospherical composites, J. Am. Chem. Soc. 125(51) (2003) 15754-15755.

[22] A. Marques, R. Reis, J. Hunt, The biocompatibility of novel starch-based polymers and composites: in vitro studies, Biomaterials 23(6) (2002) 1471-1478.

[23] M. Santander-Ortega, T. Stauner, B. Loretz, J.L. Ortega-Vinuesa, D. Bastos-González, G. Wenz, U.F. Schaefer, C.-M. Lehr, Nanoparticles made from novel starch derivatives for transdermal drug delivery, J Control Release. 141(1) (2010) 85-92.

[24] V. Bagalkot, O.C. Farokhzad, R. Langer, S. Jon, An aptamer–doxorubicin physical conjugate as a novel targeted drug□delivery platform, Angew Chem Int Ed. 45(48) (2006) 8149-8152.

[25] A. Ghaderi, M. Gholinejad, H. Firouzabadi, Palladium deposited on naturally occurring supports as a powerful catalyst for carbon-carbon bond formation reactions, Curr. Org. Chem. 20(4) (2016) 327-348.

[26] H. Tang, W. Zhao, J. Yu, Y. Li, C. Zhao, Recent development of pH-responsive polymers for cancer nanomedicine, Molecules 24(1) (2019) 4.

[27] J. Yang, L. Fan, Y. Xu, J. Xia, Iron oxide nanoparticles with different polymer coatings for photothermal therapy, J Nanopart Res. 19(10) (2017) 333.

[28] S. Mohapatra, M. Asfer, M. Anwar, S. Ahmed, F.J. Ahmad, A.A. Siddiqui, Carboxymethyl Assam Bora rice starch coated SPIONs: Synthesis, characterization and in vitro localization in a micro capillary for simulating a targeted drug delivery system, Int. J. Biol. Macromol. 115 (2018) 920-932.

[29] Y. Zhang, F. Wang, M. Li, Z. Yu, R. Qi, J. Ding, Z. Zhang, X. Chen, Self□ Stabilized Hyaluronate Nanogel for Intracellular Codelivery of Doxorubicin and Cisplatin to Osteosarcoma, Adv. Sci. 5(5) (2018) 1700821.

[30] S. Mondal, P. Manivasagan, S. Bharathiraja, M. Santha Moorthy, V.T. Nguyen, H.H. Kim, S.Y. Nam, K.D. Lee, J. Oh, Hydroxyapatite coated iron oxide nanoparticles: a promising nanomaterial for magnetic hyperthermia cancer treatment, Nanomaterials 7(12) (2017) 426.

[31] S. Mondal, U. Pal, A. Dey, Natural origin hydroxyapatite scaffold as potential bone tissue engineering substitute, Ceram. Int. 42(16) (2016) 18338-18346.

[32] H. Namduri, S. Nasrazadani, Quantitative analysis of iron oxides using Fourier transform infrared spectrophotometry, Corros. Sci. 50(9) (2008) 2493-2497.

[33] Y. Wei, B. Han, X. Hu, Y. Lin, X. Wang, X. Deng, Synthesis of Fe3O4 nanoparticles and their magnetic properties, Procedia Eng. 27 (2012) 632-637.

[34] J. Matmin, I. Affendi, S.I. Ibrahim, S. Endud, Additive-free rice starch-assisted synthesis of spherical nanostructured hematite for degradation of dye contaminant, Nanomaterials 8(9) (2018) 702.

[35] O.N. Shebanova, P. Lazor, Raman study of magnetite (Fe3O4): laser-induced thermal effects and oxidation, J Raman Spectrosc. 34(11) (2003) 845-852.

[36] K.C. Schuster, H. Ehmoser, J.R. Gapes, B. Lendl, On-line FT-Raman spectroscopic monitoring of starch gelatinisation and enzyme catalysed starch hydrolysis, Vib. Spectrosc. 22(1-2) (2000) 181-190.

[37] B. Schrader, Die Möglichkeiten der Raman□Spektroskopie im Nah□ Infrarot□Bereich, Teil II, Chem. Unserer Zeit. 31(6) (1997) 270-279.

[38] N. Santha, K. Sudha, K. Vijayakumari, V. Nayar, Moorthy, SN, Raman and infrared spectra of starch samples of sweet potato and cassava, J Chem Sci. 102(5) (1990) 705-712.

[39] E. Corbett, V. Zichy, J. Goral, C. Passingham, Fourier transform Raman studies of materials and compounds of biological importance—II. The effect of moisture on the molecular structure of the alpha and beta anomers of d-glucose, Spectrochim. Acta A Mol. Biomol. Spectrosc. 47(9-10) (1991) 1399-1411.

[40] S. Mondal, A. Dey, U. Pal, Low temperature wet-chemical synthesis of spherical hydroxyapatite nanoparticles and their in situ cytotoxicity study, Adv Nano Res. 4(4) (2016) 295.

[41] N. Mallick, M. Asfer, M. Anwar, A. Kumar, M. Samim, S. Talegaonkar, F.J. Ahmad, Rhodamine-loaded, cross-linked, carboxymethyl cellulose sodium-coated super-paramagnetic iron oxide nanoparticles: Development and in vitro localization study for magnetic drug-targeting applications, Colloids and Surfaces A: Physicochemical and Engineering Aspects 481 (2015) 51-62.

[42] P. Kumar, S. Agnihotri, I. Roy, Synthesis of dox drug conjugation and citric acid stabilized superparamagnetic iron-oxide nanoparticles for drug delivery, Biochem Physiol 5(194) (2016) 2.

[43] S. Mondal, G. Hoang, P. Manivasagan, H. Kim, J. Oh, Nanostructured hollow hydroxyapatite fabrication by carbon templating for enhanced drug delivery and biomedical applications, Ceram. Int. 45(14) (2019) 17081-17093.

[44] J. Siepmann, N.A. Peppas, Higuchi equation: derivation, applications, use and misuse, Int. J. Pharm. 418(1) (2011) 6-12.

Korean Abstract

쌀 전분 코팅 산화철 나노 입자 : 광 음향 영상 유도 광열 암 치료를 위한 치료 탐침

Vo Thi Mai Thien

4 차산업융합바이오닉스공학과, 일반대학원,

부경대학교

요약

최근 몇 년 동안, 생체 적합한 활성 물질이 코팅 된 나노 입자는 의공학 분야에서 상당한 관심을 끌고 있다. 본 연구는 광 음향 영상(PAI) 유도 화학-광열 요법으로 암을 치료하기 위해 끓인 쌀 전분 추출물(BRE)이 코팅 된 산화철 나노 입자(IONP)의 합성에 대한 실험적 연구 및 내용을 강조한다. 본 연구에서 IONP 를 합성하는데 Solvothermal 방법이 사용되었다. Physical immobilization method 는 산화철 표면에 BRE 가 로딩된 독소루비신(DOX) 분자를 코팅하는 데 역할을 한다. 체외 약물 방출은 자외선-가시 분광법을 사용하여 다양한 기간 동안 염기성 (pH 9.0), 중성 (pH 7.2) 및 산성 (pH 4.5) 조건에서 실험되었으며, 합성된 구형 BRE-IONP 의 특성 분석은 정교한 분석 기기를 사용해 진행되었다. 표적 약물 전달에서 가능한 발열 효과를 평가하기 위해 BRE-IONP 로 자기 포화 실험을 수행했으며, 생물학적 활성을 평가하기 위해 3- (4,5-dimethylthiazol-2-yl) -2,5-diphenyl tetrazolium bromide 분석 및 acridine orange / propidium iodide 형광 세포 생존력 연구가 진행되었다. BRE-IONP 는 PAI 유도 PTT 치료를 위한 높은 광열 변환 효율 (η = 29.73 %), 생체 적합성 및 높은 근적외선 영역 흡수와 함께 우수한 광열 안정성을 가진다. 본 연구는 치료 진단 응용에 적합한 생리 활성 코팅 재료로서 쌀 전분에 대한 더 나은 이해를 제공한다.

Acknowledgement

Firstly, I would like to pay my special regards to my supervisor Professor Junghwan Oh, Department of Interdisciplinary of Industry 4.0 Convergence Bionics Engineering, Pukyong National University (PKNU), he convincingly guided and encouraged me to be professional and do the right thing. It is whole-heartedly appreciated that his great advice for my study proved monumental towards the success of this study. He is the most generous and kindest teacher in my master's life. Thank you for everything you did to me, I will always memorize our time and obviously it is the strongly initial step for my whole life career.

I wish to thank all the people in my lab, thank you for being my foreign family in Korea. Thank all the people whose assistance was a milestone in the completion of this project. I'm pride in you, my friends.

I wish to show my gratitude to my family. They are always by my side and encourage me during my master's period. They are my biggest motivation to overcome the hardness in the abroad lifetime.

Finally, I wish to acknowledge the support and great love of Pukyong National University Encouragement Scholarship and Brain Korea (BK) Scholarship Program for graduate study in South Korea. Without their support and funding, this project could not have reached its goal. Their contribution is valuable and truly appreciated.

Vo Thi Mai Thien